Research Article | Vol. 25, No. 22 | 30 Oct 2017 | OPTICS EXPRESS 27283
Optics EXPRESS

Switching of the direction of reflectionless light propagation at exceptional points in non-PT-symmetric structures using phase-change materials

YIN HUANG,[1,2,*] YUECHENG SHEN,[3] CHANGJUN MIN,[2] AND GEORGIOS VERONIS[4,5]

[1]*Department of Optoelectrics Information Science and Engineering, School of Physics and Electronics, Central South University, Changsha, Hunan 410012, China*
[2]*Key Laboratory of Optoelectronic Devices and Systems of Ministry of Education and Guangdong Province, Shenzhen University, Shenzhen 518060, China*
[3]*Department of Medical Engineering, California Institute of Technology, Pasadena, CA 91125, USA*
[4]*School of Electrical Engineering and Computer Science, Louisiana State University, Baton Rouge, LA 70803, USA*
[5]*Center for Computation and Technology, Louisiana State University, Baton Rouge, LA 70803, USA*
[*]*yhuan15@csu.edu.cn*

Abstract: We introduce a non-parity-time-symmetric three-layer structure, consisting of a gain medium layer sandwiched between two phase-change medium layers for switching of the direction of reflectionless light propagation. We show that for this structure unidirectional reflectionlessness in the forward direction can be switched to unidirectional reflectionlessness in the backward direction at the optical communication wavelength by switching the phase-change material $Ge_2Sb_2Te_5$ (GST) from its amorphous to its crystalline phase. We also show that it is the existence of exceptional points for this structure with GST in both its amorphous and crystalline phases which leads to unidirectional reflectionless propagation in the forward direction for GST in its amorphous phase, and in the backward direction for GST in its crystalline phase. Our results could be potentially important for developing a new generation of compact active free-space optical devices.

OCIS codes: (260.0260) Physical optics; (350.4238) Nanophotonics and photonic crystals; (130.2790) Guided waves.

References and links

1. M. Moiseyev, *Non-Hermitian Quantum Mechanics* (Cambridge University, 2011).
2. W. D. Heiss, "Exceptional points of non-Hermitian operators," J. Phys. Math. Gen. **37**, 2455–2464 (2004).
3. W. D. Heiss, "Repulsion of resonance states and exceptional points," Phys. Rev. E **61**, 929–932 (2000).
4. A. Lupu, H. Benisty, and A. Degiron, "Switching using *PT*-symmetry in plasmonic systems: positive role of the losses," Opt. Express **21**, 21651–21668 (2013).
5. A. Lupu, H. Benisty, and A. Degiron, "Using optical *PT*-symmetry for switching applications," Photon. Nanostructures **12**, 305–311 (2014).
6. V. Achilleos, G. Theocharis, O. Richoux, and V. Pagneux, "Non-Hermitian acoustic metamaterials: Role of exceptional points in sound absorption," Phys. Rev. B **95**, 144303 (2017).
7. S. Yu, H. Park, X. Piao, B. Min, and N. Park, "Low-dimensional optical chirality in complex potentials," Optica **3**, 1025–1032 (2016).
8. M. V. Berry, "Physics of nonhermitian degeneracies," Czech. J. Phys. **54,** 1039–1047 (2004).
9. J. W. Ryu, W. S. Son, D. U. Hwang, S. Y. Lee, and S. W. Kim, "Exceptional points in coupled dissipative dynamical systems," Nano Lett. **91**, 052910 (2015).
10. O. N. Kirillov, "Exceptional and diabolical points in stability questions," Fortschr. Phys. **61**, 205–224 (2013).
11. T. Stehmann, W. S. Heiss, and F. G. Scholtz, "Observation of exceptional points in electronic circuits," J. Phys. Math. Gen. **37,** 7813–7819 (2004).
12. W. D. Heiss, "The physics of exceptional points," J. Phys. A **45**, 444016 (2012).
13. C. M. Bender and S. Boettcher, "Real spectra in non-Hermitian Hamiltonians having *PT*-symmetry," Phys. Rev. Lett. **80**, 5243 (1998).

#307118 https://doi.org/10.1364/OE.25.027283
Journal © 2017 Received 13 Sep 2017; revised 11 Oct 2017; accepted 18 Oct 2017; published 23 Oct 2017

Optics EXPRESS

14. Z. Lin, H. Ramezani, T. Eichelkraut, T. Kottos, H. Cao, and D. N. Christodoulides, "Unidirectional invisibility induced by PT-symmetric periodic structures," Phys. Rev. Lett. **106**, 213901 (2011).
15. A. Regensburger, C. Bersch, M. A. Miri, G. Onishchukov, D. N. Christodoulides, and U. Peschel, "Parity-time synthetic photonic lattices," Nature **488**, 167–171 (2012).
16. L. Ge, Y. D. Chong, and A. D. Stone, "Conservation relations and anisotropic transmission resonances in one-dimensional PT-symmetric photonic heterostructures," Phys. Rev. A **85**, 023802 (2012).
17. Y. Huang, Y. Shen, C. Min, S. Fan, and G. Veronis, "Unidirectional reflectionless light propagation at exceptional points," Nanophotonics **6**, 977–996 (2017).
18. X. Yin and X. Zhang, "Unidirectional light propagation at exceptional points," Nat. Mater. **12**, 175–177 (2013).
19. L. Feng, Y. L. Xu, W. S. Fegadolli, M. H. Lu, J. E. B. Oliveira, V. R. Almeida, Y. F. Chen, and A. Scherer, "Experimental demonstration of a unidirectional reflectionless parity-time metamaterial at optical frequencies," Nat. Mater. **12**, 108–113 (2013).
20. L. Feng, X. Zhu, S. Yang, H. Zhu, P. Zhang, X. Yin, Y. Wang, and X. Zhang, "Demonstration of a large-scale optical exceptional point structure," Opt. Express **22**, 1760–1767 (2014).
21. Y. Shen, X. H. Deng, and L. Chen, "Unidirectional invisibility in a two-layer non-PT-symmetric slab," Opt. Express **22**, 19440–19447 (2014).
22. B. Peng, S. K. Ozdemir, M. Liertzer, W. Chen, K. Johannes, H. Yilmaz, J. Wiersig, Rotter. S, and L. Yang, "Chiral modes and directional lasing at exceptional points," Proc. Natl. Acad. Sci. USA **113**, 6845–6850 (2016).
23. Y. Huang, G. Veronis, and C. Min, "Unidirectional reflectionless propagation in plasmonic waveguide-cavity systems at exceptional points," Opt. Express **23**, 29882–29895 (2015).
24. Y. Jia, Y. Yan, S. V. Kesava, Z. D. Gomez, and N. C. Giebink, "Passive parity-time symmetry in organic thin film waveguides," ACS Photonics **2**, 319–325 (2015).
25. S. A. R. Horsley, M. Artoni, and G. C. La Rocca, "Spatial Kramer-Kronig relations and the reflection of waves," Nat. Photonics **9**, 436–439 (2015).
26. Y. Huang, C. Min, and G. Veronis, "Broadband near total light absorption in non-PT-symmetric waveguide-cavity systems," Opt. Express **24**, 22219–22231 (2016).
27. E. Yang, Y. Lu, Y. Wang, Y. Dai, and P. Wang, "Unidirectional reflectionless phenomenon in periodic ternary layered material," Opt. Express **24**, 14311–14321 (2016).
28. S. Yu, X. Piao, and N. Park, "Acceleration toward polarization singularity inspired by relativistic E×B drift," Sci. Rep. **6**, 37754 (2016).
29. S. Yu, X. Piao, K. Yoo, J. Shin, and N. Park, "One-way optical modal transition based on causality in momentum space," Opt. Express **23**, 24997–25008 (2015).
30. S. Longhi, "Bidirectional invisibility in Kramers-Kronig optical media," Opt. Lett. **41**, 2727–2730 (2016).
31. X. Li, Q. Tan, B. Bai, and G. Jin, "Experimental demonstration of tunable directional excitation of surface plasmon polaritons with a subwavelength metallic double slit," Appl. Phys. Lett. **98**, 251109 (2011).
32. J. Lin, J. B. Mueller, Q. Wang, G. Yuan, N. Antoniou, X. Yuan, and F. Capasso, "Polarization-controlled tunable directional coupling of surface plasmon polaritons," Science **340**, 331–334 (2013).
33. S. Kim, H. Yun, K. Park, J. Hong, J. Yun, K. Lee, J. Kim, S. Jeong, S. Mun, J. Sung, Y. Lee, and B. Lee, "Active directional switching of surface plasmon polaritons using a phase transition material," Sci. Rep. **7**, 43723 (2017).
34. K. Shportko, S. Kremers, M. Woda, D. Lencer, J. Robertson, and M. Wuttig, "Resonant bonding in crystalline phase-change materials," Nat. Mater. **7**, 653–658 (2008).
35. M. Rude, V. Mkhitaryan, A. E. Cetin, T. A. Miller, A. Carrilero, S. Wall, F. J. Abajo, H. Altug, and V. Pruneri, "Ultrafast and broadband tuning of resonant optical nanostructures using phase-change materials," Adv. Optical Mater. **4**, 1060–1066 (2016).
36. D. Loke, T. H. Lee, W. J. Wang, L. P. Shi, R. Zhao, Y. C. Yeo, C. T. Chong, and S. R. Elliott, "Breaking the speed limits of phase-change memory," Science **336**, 1556–1569 (2012).
37. T. Hira, T. Homma, T. Uchiyama, K. Kuwamura, Y. Kihara, and T. Saiki, "All-optical switching of localized surface plasmon resonance in single gold nanosandwich using GeSbTe film as an active medium," Appl. Phys. Lett. **106,** 031105 (2015).
38. M. Wuttig and N. Yamada, "Phase-change materials for rewriteable data storage," Nat. Mater. **6**, 824–832 (2007).
39. M. H. R. Lankhorst, B. W. Ketelaarsand, and R. A. M. Wolters, "Low-cost and nanoscale non-volatile memory concept for future silicon chips," Nat. Mater. **4**, 347–352 (2005).
40. F. F. Schlich, P. Zalden, A. M. Lindenberg, and R. Spolenak, "Color switching with enhanced optical contrast in ultrathin phase change materials and semiconductors induced by femtosecond laser pulses," ACS Photonics **2**, 178–182 (2015).
41. M. Rude, R. E. Simpson, R. Quidant, V. Pruneri, and J. Renger, "Active control of surface plasmon waveguides with a phase change material," ACS Photonics **2**, 669–674 (2015).
42. Q. Wang, E. T. F. Rogers, B. Gholipour, C. Wang, G.Yuan, J. Teng, N. I. Zheludev, "Optically reconfigurable metasurfaces and photonic devices based on phase change materials," Nat. Photonics **10**, 60–65 (2016).
43. P. Li, X. Yang, T. W. W. Mab, J. Hanss, M. Lewin, A. U. Michel, M. Wuttig, and T. Taubner, "Reversible optical switching of highly confined phonon-polaritons with an ultrathin phase-change material," Nat. Mater. **15**, 870–876 (2016).
44. V. K. Mkhitaryan, D. S. Ghosh, M. Rude, J. Canet-Ferrer, R. A. Maniyara, K. K. Gopalan, and V. Pruneri, "Tunable

Optics EXPRESS

complete optical absorption in multilayer structures including $Ge_2Sb_2Te_5$ without lithographic patterns," Adv. Optical Mater. **5**, 1600452 (2017).
45. S. Yoo, T. Gwon, T. Eom, S. Kim, and C. Hwang, "Multicolor changeable optical coating by adopting multiple layers of ultrathin phase change material film," ACS Photonics **3**, 1265–1270 (2016).
46. S. Phang, A. Vukovic, H. Susanto, T. M. Benson, and P. Sewell, "Ultrafast optical switching using PT-symmetric Bragg gratings," J. Opt. Soc. Am. B **30**, 2984–2991 (2014).
47. S. Fan, R. Baets, A. Petrov, Z.Yu, J. D. Joannopoulos, W. Freude, A. Melloni, M. Popovic, M. Vanwolleghem, D. Jalas, M. Eich, M. Krause, H. Renner, E. Brinkmeyer, and C. R. Doerr, "Comment on 'Nonreciprocal light propagation in a silicon photonic circuit'," Science **335**, 38 (2012).
48. H. A. Haus, *Waves and Fields in Optoelectronics* (Prentice-Hall, 1984).
49. A. Yariv and P. Yeh, *Optical Electronics in Modern Communications* (Oxford University, 2007).
50. G. Veronis, R. W. Dutton, and S. Fan, "Method for sensitivity analysis of photonic crystal devices," Opt. Lett. **29,** 2288–2290 (2004).
51. J. Jin, *The Finite Element Method in Electromagnetics* (Wiley, 2002).
52. A. Taflove, *Computational Electrodynamics* (Artech House, 1995).
53. V. E. Babicheva, I. V. Kulkova, R. Malureanu, K. Yvind, and A. V. Lavrinenko, "Plasmonic modulator based on gain-assisted metal-semiconductor-metal waveguide," Photon. Nanostructures **10,** 389–399 (2012).
54. M. Levinshtein, S. Rumyantsev, and M. Shur, *Handbook Series on Semiconductor Parameters* (World Scientific, 1999).
55. E. U. Rafailov, M. A. Cataluna, and W. Sibbett, "Mode-locked quantum-dot lasers," Nat. Photonics. **1**, 395–401 (2007).
56. K. Kawaguchi, N. Yasuoka, M. Ekawa, H. Ebe, T. Akiyama, M. Sugawara, and Y. Arakawa, "Demonstration of transverse-magnetic dominant gain in quantum dot semiconductor optical amplifiers," Appl. Phys. Lett. **93,** 121908 (2008).
57. E. S. Semenova, I. V. Kulkova, S. Kadkhodazadeh, M. Schubert, and K. Yvind, "Metal organic vapor-phase epitaxy of InAs/InGaAsP quantum dots for laser applications at 1.5 μm," Appl. Phys. Lett. **99,** 101106 (2011).
58. M. A. Kats, D. Sharma, J. Lin, P. Genevet, R. Blanchard,Z. Yang, M. M. Qazilbash, D. N. Basov, S. Ramanathan, and F. Capasso, "Ultra-thin perfect absorber employing a tunable phase change material," Appl. Phys. Lett. **101,** 221101 (2012).
59. M. A. Kats, R. Blanchard, P. Genevet, and F. Capasso, "Nanometre optical coatings based on strong interference effects in highly absorbing media," Nat. Mater. **12**, 20–24 (2013).
60. M. P. Nezhad, K. Tetz, and Y. Fainman, "Gain assisted propagation of surface plasmon polaritons on planar metallic waveguides," Opt. Express **12,** 4072–4079 (2004).
61. D. Bimberg, N. N. Ledentsov, M. Grundmann, F. Heinrichsdorff, V. M. Ustinov, P. S. Kopev, Z. I. Alferov, and J. A. Lott, "Edge and vertical cavity surface emitting InAs quantum dot lasers," Solid St. Electron. **42,** 1433–1437 (1998).
62. N. Kirstaedter, O. G. Schmidt, N. N. Ledentsov, D. Bimberg, V. M. Ustinov, A. Yu. Egorov, A. E. Zhukov, M. V. Maximov, P. S. Kopev, and Zh. I. Alferov, "Gain and differential gain of single layer InAs/GaAs quantum dot injection lasers," Appl. Phys. Lett. **69,** 1226–1228 (1996).
63. K. Akahane, N. Ohtani, Y. Okada, and M. Kawabe, "Fabrication of ultra-high density InAs-stacked quantum dots by strain-controlled growth on InP(3 1 1)B substrate," J. Cryst. growth **245,** 31–36 (2002).
64. K. Akahane, N. Yamamoto, and T. Kawanishi, "Fabrication of ultra-high-density InAs quantum dots using the strain-compensation technique," Phys. Status Solidi A **208,** 425–428 (2011).
65. C. Dembowski, H. Graf, H. L. Harney, A. Heine, W. D. Heiss, H. Rehfeld, and A. Richter, "Experimental observation of the topological structure of exceptional points," Phys. Rev. Lett. **86,** 787–790 (2001).
66. B. Zhen, C. W. Hsu, Y. Igarashi, L. Lu, I. Kaminer, A. Pick, S. Chua, J. D. Joannopoulos. and M. Soljacic, "Spawning rings of exceptional points out of Dirac cones," Nature **525,** 354–358 (2015).
67. J. Doppler, A. A. Mailybaev, J. Bohm, U. Kuhl, A. Girschik, F. Libisch, T. J. Milburn, P. Rabl, N. Moiseyev, and S. Rotter, "Dynamically encircling an exceptional point for asymmetric mode switching," Nature **537,** 76–80 (2016).
68. Q. Liu, B. Wang, S. Ke, H. Long, K. Wang, and P. Lu, "Exceptional points in Fano-resonant graphene metamaterials," Opt. Express **25**, 7203–7212 (2017).

1. Introduction

Exceptional points, which are branch point singularities of the spectrum, are associated with the coalescence of both eigenvalues and corresponding eigenstates in open quantum systems described by non-Hermitian Hamiltonians [1-7]. Exceptional points have been studied in lasers [8], coupled dissipative dynamical systems [9], mechanics [10], electronic circuits [11], and atomic as well as molecular systems [12]. In the past few years, unidirectional light reflectionlessness caused by the existence of exceptional points in non-Hermitian parity-time (PT) symmetric optical systems possessing balanced gain and loss has attracted considerable attention [13-17]. In such structures the reflection is zero when measured from one end of the structure at optical exceptional points,

Optics EXPRESS

and nonzero when measured from the other end. Unidirectional light reflectionlessness can also be attained in non-*PT*-symmetric structures with unbalanced gain and loss [18-30]. This is due to the fact that exceptional points exist in a larger family of non-Hermitian Hamiltonians [18]. Achieving unidirectional reflectonless propagation is important for several key applications in photonic circuits such as optical network analyzers [15, 19]. In addition, switching of the direction of reflectionless light propagation could be essential for building compact optoelectronic devices, for reducing the size of optical systems, and for developing reconfigurable optical components [31–33]. This could be achieved by using materials with tunable optical properties such as phase-change materials.

$Ge_2Sb_2Te_5$ (GST) is a phase-change material with amorphous and crystalline phases [34]. The atom distribution of GST is chaotic in the amorphous phase. In contrast, the atoms are aligned in an orderly manner in the crystalline phase. Thus, GST can significantly change its optical properties through phase transitions. GST can be switched reversibly and rapidly between its amorphous and crystalline phases by applying external electrical pulses, optical pulses or thermal annealing. Picosecond-order crystallization times have been reported for GST by femtosecond laser pulses [35,36]. Amorphization of GeSbTe has been achieved on the subpicosecond timescale with femtosecond laser pulse excitation [37]. In addition, GST retains its phase for years after removal of the external excitations. GST has been widely studied for applications in non-volatile, rewritable optical data storage and memory [38,39]. Recently, a variety of optically reconfigurable GST-based active photonic devices have also been demonstrated [40-45].

In this paper, motivated by the transport behavior enabled by non-Hermiticity and the high refractive index contrast between the amorphous and crystalline phases of phase-change material GST, we use a non-*PT*-symmetric three-layer structure, consisting of a gain medium layer sandwiched between two GST layers, to switch the direction of reflectionless light propagation at exceptional points. We show that, when GST is switched from its amorphous to its crystalline phase, the structure switches from unidirectional reflectionless in the forward direction to unidirectional reflectionless in the backward direction. The structure is designed at the optical communication wavelength of $\lambda_0 = 1.55\mu$m. We then discuss the underlying physical mechanism of unidirectional reflectionless light propagation in this structure. We show that a layer with gain has to be included in the structure to compensate the loss in the GST layers so as to achieve complete destructive interference. We demonstrate that the structure exhibits exceptional points for GST in both its amorphous and crystalline phases. These exceptional points result in unidirectional reflectionless propagation in the forward direction for GST in its amorphous phase, and in the backward direction for GST in its crystalline phase. We investigate the phase transitions associated with the exceptional points. Finally, the topological structure of the exceptional points is also explored by encircling them in parameter space.

The remainder of the paper is organized as follows. In Section 2, we briefly review unidirectional reflectionless light propagation at exceptional points. In Subsection 3.1, we use the three-layer structure, consisting of a gain medium layer sandwiched between two GST layers, to realize switching of the direction of reflectionless light propagation. In Subsection 3.2, we investigate the exceptional points of the structure which lead to unidirectional reflectionless propagation and their topological properties. Finally, our conclusions are summarized in Section 4.

2. Theory

Our proposed structure consists of a gain medium layer sandwiched between two GST layers (Fig. 1). The optical properties of our proposed system can be described by the scattering matrix **S** defined by the following equation [14, 16, 17, 20, 46–48]

$$\begin{pmatrix} H_R^- \\ H_L^- \end{pmatrix} = \mathbf{S} \begin{pmatrix} H_L^+ \\ H_R^+ \end{pmatrix} = \begin{pmatrix} t & r_b \\ r_f & t \end{pmatrix} \begin{pmatrix} H_L^+ \\ H_R^+ \end{pmatrix}, \tag{1}$$

Optics EXPRESS

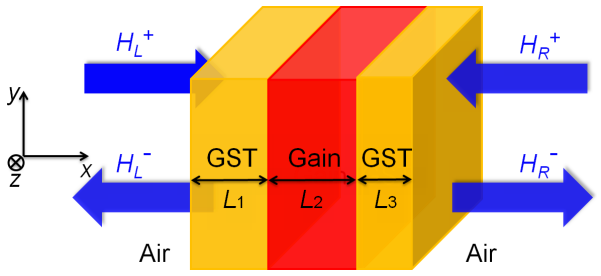

Fig. 1. Schematic of a non-*PT*-symmetric three-layer structure composed of a gain medium layer sandwiched between two GST layers for switching of the direction of reflectionless light propagation at exceptional points.

where H_L^+, and H_R^+ are the complex magnetic field amplitudes of the incoming waves at the left and right ports, respectively. Similarly, H_L^-, and H_R^- are the complex magnetic field amplitudes of the outgoing waves from the left and right ports, respectively. In addition, t is the complex transmission coefficient, while r_f, r_b are the complex reflection coefficients for uniform plane waves normally incident from the left (forward direction) and from the right (backward direction), respectively. In general, the matrix $\mathbf{S}$ is non-Hermitian, and its complex eigenvalues are $\lambda_s^{\pm} = t \pm \sqrt{r_f r_b}$. Its eigenstates, which are $\psi_{\pm} = (\sqrt{r_b}, \pm\sqrt{r_f})^T$, are not orthogonal. In our proposed three-layer optical system (Fig. 1), by manipulating the elements of the scattering matrix, the two eigenvalues can be coalesced and form exceptional points. This leads to unidirectional reflectionless propagation in either the forward ($r_f = 0, r_b \neq 0$) or the backward ($r_b = 0, r_f \neq 0$) direction. We use the transfer matrix method to calculate t, r_f, and r_b for the three-layer structure of Fig. 1 [49].

When the system includes loss or gain, while the transmission coefficients in the forward and backward directions are the same, the reflection coefficients in the forward and backward directions are in general different. Such a system is analogous to open quantum systems which are characterized by complex non-Hermitian Hamiltonians [16-19, 22]. We will show that switching of the direction of reflectionless light propagation at exceptional points at the wavelength of 1.55 μm can be achieved by proper tuning of the geometric and material parameters of the structure of Fig. 1. More specifically, unidirectional reflectionlessness in the forward direction ($r_f = 0, r_b \neq 0$) can be switched to unidirectional reflectionlessness in the backward direction ($r_b = 0, r_f \neq 0$) by switching the phase-change material GST from its amorphous to its crystalline phase.

3. Results

In this section, we use a non-*PT*-symmetric three-layer structure, consisting of a gain medium layer sandwiched between two GST layers (Fig. 1), to realize switching of the direction of reflectionless light propagation as discussed in the previous section. We found that both GST layers are critical for realizing the switching. More specifically, we first investigated a two-layer structure consisting of a gain medium layer and a single GST layer. We found that such a two-layer structure cannot be optimized to achieve the same functionality. We use the finite-difference frequency-domain (FDFD) method [50] to numerically calculate the reflection coefficients in the proposed structure. Perfectly matched layer (PML) absorbing boundary conditions are used at all boundaries of the simulation domain [51]. We also use the total-field-scattered-field (TFST) formulation to simulate the response of the structure to a normally incident plane wave input [52].

3.1. Switching of the direction of reflectionless light propagation

To realize switching of the direction of reflectionless light propagation, we use the transfer matrix method as described in Section 2. More specifically, we optimize the thicknesses of all three

Optics EXPRESS

layers L_1, L_2, and L_3 (Fig. 1), as well as the imaginary part k of the refractive index $\tilde{n}_g$ of the gain material, to make the sum of the amplitude of the reflection coefficient in the forward direction $|r_f|$ as close to zero as possible while of the amplitude of the reflection coefficient in the backward direction $|r_f|$ as large as possible when GST is in its amorphous phase, and make the sum of the amplitude of the reflection coefficient in the backward direction $|r_b|$ as close to zero as possible while of the amplitude of the reflection coefficient in the forward direction $|r_f|$ as large as possible when GST is in its crystalline phase at the optical communication wavelength of $\lambda_0 = 1.55\mu$m. We use experimental data for the frequency-dependent dielectric constant of amorphous GST (aGST) and crystalline GST (cGST) [34]. The refractive indices of aGST and cGST are $\tilde{n}_{\text{aGST}} = 4.7 + j0.2$ and $\tilde{n}_{\text{cGST}} = 7 + j2$, respectively, at $\lambda_0 = 1.55\mu$m [34, 35]. In the presence of pumping, optical gain can be achieved using InGaAsP with InAs quantum dots (QDs) [53–57]. The real part of the refractive index for $\text{In}_x\text{Ga}_{1-x}\text{As}_y\text{P}_{1-y}$ in the infrared is given by $n = 3.1 + 0.46y$ [53, 54], and is weakly dependent on the wavelength [53, 54]. Here, we assume that the real part of the refractive index of the gain material is 3.44. Since the transfer matrix method (Section 2) for the structure of Fig. 1 is computationally very efficient, we are able to use an exhaustive search in the design parameter space (L_1, L_2, L_3, and k) to optimize the structure. Using this approach, we find that for $L_1 = 276$ nm, $L_2 = 84$ nm, $L_3 = 2$ nm, and $k = -0.67$ the reflection in the backward direction is almost zero ($R_b = |r_b|^2 \simeq 3.4820 \times 10^{-7}$) when GST is in its crystalline phase, and the reflection in the forward direction is also almost zero ($R_f = |r_f|^2 \simeq 7.1352 \times 10^{-5}$) when GST is in its amorphous phase at $\lambda_0 = 1.55\mu$m. In addition, the reflection in the forward direction when GST is in its crystalline phase is nonzero ($R_f = |r_f|^2 \simeq 0.743$), and the reflection in the backward direction when GST is in its amorphous phase is nonzero ($R_b = |r_b|^2 \simeq 0.5896$) as well. Thus, we conclude that for the structure of Fig. 1 switching of the direction of reflectionless light propagation can be realized at the optical communication wavelength by switching the phase-change material GST between its amorphous and crystalline phases.

Figure 2(a) shows the reflection spectra for the structure of Fig. 1 with GST in its crystalline phase calculated for both forward and backward directions using full-wave FDFD simulations for $L_1 = 276$ nm, $L_2 = 84$ nm, $L_3 = 2$ nm, and $k = -0.67$. The FDFD results confirm that the optimized structure of Fig. 1 with GST in its crystalline phase is unidirectional reflectionless at $f = 193.4$ THz ($\lambda_0 = 1.55\mu$m), since the reflection in the backward direction R_b is zero, while the reflection in the forward direction R_f is nonzero. We note that for all the structures investigated in this paper the transfer matrix method results are in excellent agreement with the FDFD results. In addition, the contrast ratio between the forward and backward reflection, defined as $\eta = |\frac{R_f - R_b}{R_f + R_b}|$ [19], as a function of frequency is shown in Fig. 2(b). At the wavelength of $\lambda_0 = 1.55\mu$m, the contrast ratio almost reaches unity ($\eta \simeq 0.9999$). The unidirectional reflectionless propagation can be observed in the magnetic field distributions for $L_1 = 276$ nm, $L_2 = 84$ nm, $L_3 = 2$ nm, and $k = -0.67$ [Figs. 2(c)-2(f)]. When the plane wave is normally incident from the left (forward direction), the field decays significantly in the left GST layer due to strong absorption, and the incident and reflected waves in air form a strong interference pattern [Figs. 2(c) and 2(e)]. On the other hand, when the uniform plane wave is incident from the right (backward direction), the maximum field is at the interface between the left GST layer and the gain medium layer within the structure, and there is hardly any reflection due to the complete destructive interference between all the reflected waves at the right boundary of the structure [Figs. 2(d) and 2(f)]. Note that the bulk refractive index of GST that we used here is still valid for the ultrathin GST layer with 2 nm thickness [40, 45].

Figure 3(a) shows the reflection spectra for the structure of Fig. 1 with GST in its amorphous phase calculated for both forward and backward directions using full-wave FDFD simulations for $L_1 = 276$ nm, $L_2 = 84$ nm, $L_3 = 2$ nm, and $k = -0.67$. The FDFD results also confirm that the optimized structure of Fig. 1 with GST in its amorphous phase is unidirectional reflectionless at

Optics EXPRESS

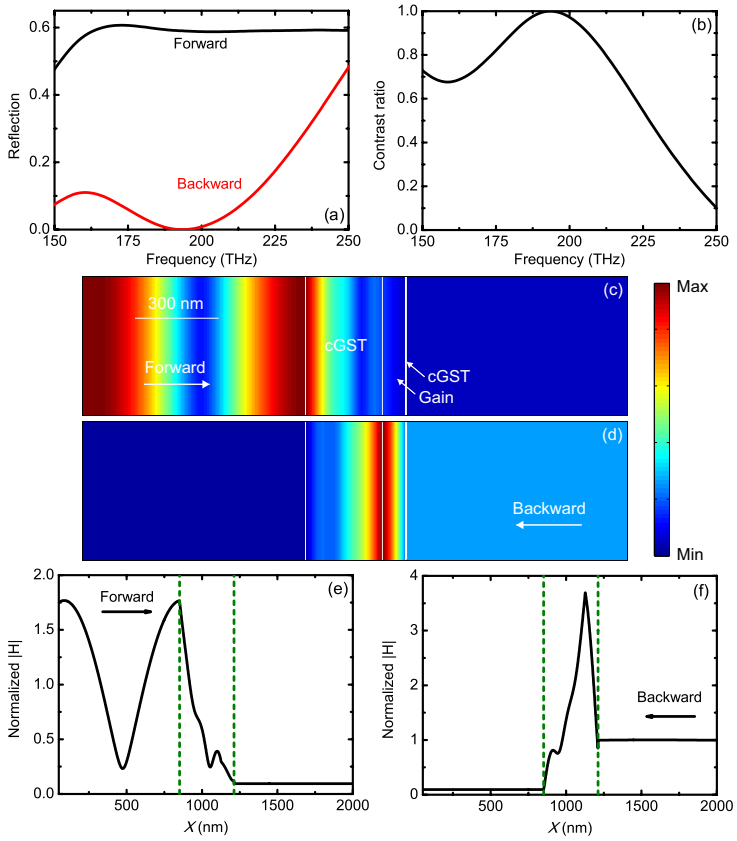

Fig. 2. (a) Reflection spectra for the optimized structure of Fig. 1 with GST in its crystalline phase calculated for normal incidence from both the forward and backward directions using FDFD. Results are shown for L_1 = 276 nm, L_2 = 84 nm, and L_3 = 2 nm. The gain medium is InGaAsP with InAs QDs ($\tilde{n}_g = n + jk$ = 3.44 - j0.67). (b) Contrast ratio spectra for the optimized structure of Fig. 1 with GST in its crystalline phase. All parameters are as in Fig. 2(a). (c) and (d) Magnetic field amplitude profiles for the optimized structure of Fig. 1 with GST in its crystalline phase at f = 193.4 THz (λ_0 =1.55μm), when a plane wave is normally incident from the left and right, respectively. All other parameters are as in Fig. 2(a). (e) and (f) Magnetic field amplitude in the optimized structure of Fig. 1 with GST in its crystalline phase at f = 193.4 THz (λ_0 =1.55μm), normalized with respect to the field amplitude of the incident plane wave, when the light is incident from the left and right, respectively. The two vertical dashed lines indicate the left boundary of the left GST layer, and the right boundary of the right GST layer. All other parameters are as in Fig. 2(a).

f = 193.4 THz (λ_0 = 1.55μm), since the reflection in the forward direction R_f is zero, while the reflection in the backward direction R_b is nonzero. The contrast ratio between the forward and backward reflection as a function of frequency is shown in Fig. 3(b). At the wavelength of λ_0 = 1.55μm, the contrast ratio almost reaches unity ($\eta \simeq$0.9999). Similarly, the unidirectional reflectionless propagation can be observed in the magnetic field distributions for L_1 = 276 nm, L_2 = 84 nm, L_3 = 2 nm, and k = −0.67 [Figs. 3(c)-3(f)]. When the plane wave is normally incident from the right (backward direction), the incident and reflected waves in air form a strong interference pattern [Figs. 3(d) and 3(f)]. On the other hand, when the uniform plane wave is normally incident from the left (forward direction), there is hardly any reflection due to the complete destructive interference between all the reflected waves at the left boundary of the

Optics EXPRESS

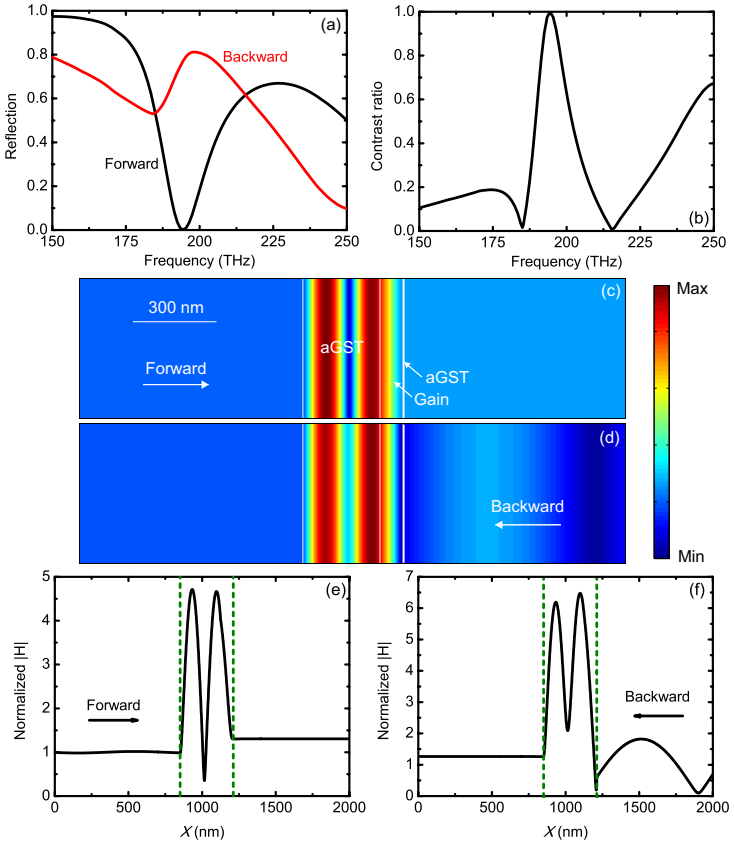

Fig. 3. (a) Reflection spectra for the optimized structure of Fig. 1 with GST in its amorphous phase calculated for normal incidence from both the forward and backward directions using FDFD. All parameters are as in Fig. 2(a). (b) Contrast ratio spectra for the optimized structure of Fig. 1 with GST in its amorphous phase. All parameters are as in Fig. 2(a). (c) and (d) Magnetic field amplitude profiles for the optimized structure of Fig. 1 with GST in its amorphous phase at f = 193.4 THz (λ_0 =1.55μm), when a plane wave is normally incident from the left and right, respectively. All other parameters are as in Fig. 2(a). (e) and (f) Magnetic field amplitude in the optimized structure of Fig. 1 with GST in its amorphous phase at f = 193.4 THz (λ_0 =1.55μm), normalized with respect to the field amplitude of the incident plane wave, when the light is incident from the left and right, respectively. The two vertical dashed lines indicate the left boundary of the left GST layer, and the right boundary of the right GST layer. All other parameters are as in Fig. 2(a).

structure [Figs. 3(c) and 3(e)].

As we saw above, in the optimized structure the thickness of the right GST layer L_3 is only 2 nm, which is much smaller than the wavelength of light λ_0 = 1.55 μm. In general, there is hardly any phase shift in a few nm thick layer. However, if we remove this ultrathin layer from the optimized structure of Fig. 1 with GST in its crystalline phase, the reflection in the backward direction increases significantly from 0 to 5.6%. This is due to the large extinction coefficient of cGST, as we will see below. In fact, if this ultrathin layer has an even higher extinction coefficient, the difference between the reflections from the structure with and without the ultrathin layer will be even larger. As an example, at the frequency of f = 250 THz, GST in its crystalline phase has a higher extinction coefficient (the refractive index is 6.45 + j3.0), compared to that at f = 193.4 THz (λ_0 = 1.55 μm). Thus, at the frequency of f = 250 THz the reflection in the backward

Optics EXPRESS

direction dramatically changes from 48.8% to 76.2%, if the 2 nm GST layer is removed from the optimized structure.

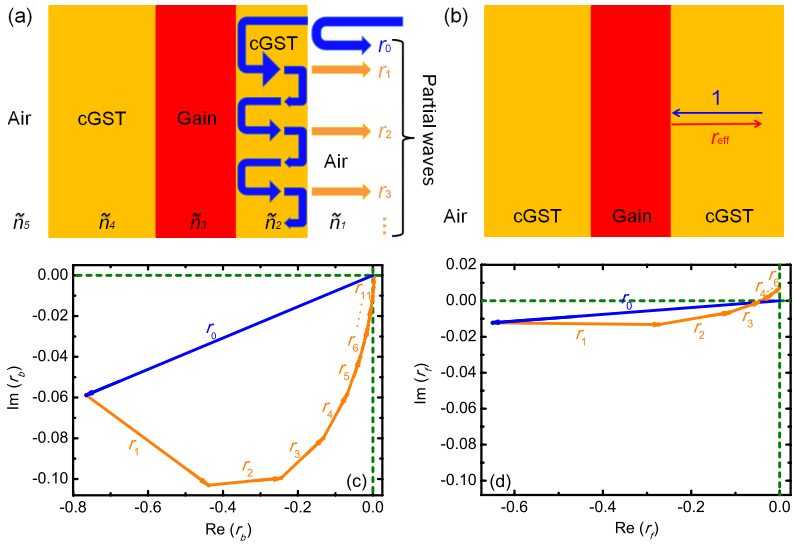

Fig. 4. (a) The reflection process at normal incidence from a three-layer structure composed of a gain medium layer sandwiched between two GST layers showing the partial waves. GST is in its crystalline phase. (b) Schematic defining the reflection coefficient r_{eff} when a plane wave is normally incident on the boundary between GST and a two-layer structure composed of a gain medium layer and a GST layer above an air substrate. GST is in its crystalline phase. (c) Phasor diagram demonstrating that a zero-reflection condition is achievable via destructive interference for the optimized structure of Fig. 1 with GST in its crystalline phase. A plane wave is incident from the right (backward direction) at f = 193.4 THz (λ_0 =1.55 μm). All other parameters are as in Fig. 2(a). (d) Phasor diagram demonstrating that a zero-reflection condition is achievable via destructive interference for the structure of Fig. 1 with GST in its amorphous phase. A plane wave is incident from the left (forward direction) at f = 193.4 THz. All other parameters are as in Fig. 2(a).

We further investigate the role of the ultrathin cGST layer with thickness L_3 in the reflection process from the three-layer structure of Fig. 1. The ultrathin layer can be regarded as a cavity between air and the gain-cGST-air structure [Fig. 4(a)]. The total reflected wave in the backward direction can be calculated as the coherent sum of the partial wave reflected from the interface between air and cGST with reflection coefficient r_0, and those reflected from the 2 nm ultrathin cGST layer after one, two, three, ... roundtrips with reflection coefficients r_1, r_2, r_3, ... [Fig. 4(a)]. The total reflection coefficient in the backward direction r_b can then be obtained as [58]

$$r_b = \sum_{m=0}^{\infty} r_m = \frac{r_{12} + r_{\text{eff}} e^{2j\gamma L_3}}{1 + r_{12} r_{\text{eff}} e^{2j\gamma L_3}}, \tag{2}$$

where $r_m = t_{12} r_{\text{eff}}^m r_{21}^{m-1} t_{21} e^{2j\gamma L_3}$ for $m > 0$. Here $r_{pq} = \frac{\tilde{n}_p - \tilde{n}_q}{\tilde{n}_p + \tilde{n}_q}$, $t_{pq} = \frac{2\tilde{n}_p}{\tilde{n}_p + \tilde{n}_q}$ are the Fresnel reflection and transmission coefficients when a plane wave is normally incident on medium q from medium p [49], $\tilde{n}_p$ is the complex refractive index of medium p, $r_0 = r_{12}$, and $\gamma = \frac{2\pi\tilde{n}_2}{\lambda_0}$. Here, $\tilde{n}_1 = \tilde{n}_5 = 1$, $\tilde{n}_2 = \tilde{n}_4 = \tilde{n}_{\text{cGST}}$, and $\tilde{n}_3 = \tilde{n}_g$ [Fig. 4(a)]. Finally, r_{eff} is the complex reflection coefficient when a plane wave is normally incident on the boundary between cGST and a two-layer structure composed of a gain medium layer and a cGST layer above an air substrate [Fig. 4(b)].

Optics EXPRESS

In Fig. 4(c), we show a phasor diagram, in which the reflected partial waves are plotted in the complex plane, to describe the reflection property in the backward direction of the optimized three-layer structure of Fig. 1 with GST in its crystalline phase. The sum of the reflected partial waves, r_m, after m round trips in the ultrathin cGST layer destructively interferes with the first partial wave reflected from the interface between air and cGST, r_0. In the case of lossless dielectrics, phase accumulation occurs when light propagates through the layer. Light reflected at an interface between two lossless dielectrics can induce either π or 0 phase shifts [49]. However, when at least one of the dielectrics has a large extinction coefficient, the reflection coefficient is complex. The interface reflection can contribute a phase shift which is neither π nor 0, so that it is not necessary to achieve large phase accumulation via propagation through a thick dielectric layer as in the lossless case [58,59]. Thus, due to the large extinction coefficient of cGST, a strong phase accumulation can be achieved by the ultrathin cGST layer, and the overall destructive interference leads to a zero reflection in the backward direction. The phasor path traces out a loop in the complex plane far from the horizontal axis, due to the large extinction coefficient of cGST, but returns to the origin since the destructive interference is complete [Fig. 4(c)].

In Fig. 4(d), we show a phasor diagram to describe the reflection property in the forward direction of the optimized three-layer structure of Fig. 1 with GST in its amorphous phase, based on the same method used in Fig. 4(c). All reflected partial waves destructively interfere almost completely, so that the phasor path returns to a point very close to the origin [Fig. 4(d)]. In the case of lossless dielectrics, the phasor trajectory is along the horizontal axis [58,59]. Even though the phasor trajectory shown in Fig. 4(d) still traces out a loop in the complex plane due to loss in aGST, unlike the previous case of cGST [Fig. 4(c)], the loop path is very close to the horizontal axis because of the small extinction coefficient of aGST. Since aGST has a small extinction coefficient, the reflection in the forward direction remains close to zero even if we remove the ultrathin right aGST layer. On the other hand, the left aGST layer has to be thick enough (L_1 = 276 nm) to achieve sufficient phase shift for substantial destructive interference.

Figure 5(a) shows the reflection in the backward direction for the optimized structure with GST in its crystalline phase as a function of the real and imaginary parts of the complex refractive index of the gain medium. Similarly, Fig. 5(b) shows the reflection in the forward direction for the optimized structure with GST in its amorphous phase. We observe that the material of the middle layer has to exhibit gain ($k < 0$) in order to realize zero reflection in the backward direction ($R_b = 0$) for GST in its crystalline phase, and zero reflection in the forward direction ($R_f = 0$) for GST in its amorphous phase. This is because, in the absence of gain, each reflected partial wave would be highly attenuated after light propagates several round trips through the lossy GST layers, and the sum of reflection coefficients r_1, r_2, r_3, ... would not cancel out the primary reflection coefficient r_0. Thus, gain material has to be used in our optimized structure in order to compensate the material loss in the GST layers and achieve complete destructive interference. Note that the imaginary part of the refractive index of the gain material used in the optimized structure is 0.67, which corresponds to a gain coefficient of g$\approx$ 47580 cm^{-1} [60]. Also note that the near zero reflection regime is broad in the $n - k$ space [Figs. 5(a) and 5(b)], which relaxes the requirements for realization of our proposed structures. In recent related experiments on unidirectional reflectionless structures the measured contrast ratio was 70% [19]. We found that our proposed structures can have contrast ratios of at least 70% using a significantly lower material gain of $\sim$ 32000 cm^{-1}. Even though achieving the material gain required for our design is challenging, it could be realized with QDs. QDs exhibit exceptionally large material gain [61,62]. In addition, structures with ultra-high-density QDs and therefore very large QDs volume ratio have been recently reported [63,64]. Such ultra-high-density QD structures could achieve the material gain required for our design. We finally note that the required material gain coefficient can be greatly reduced if the thickness of the gain medium layer is increased. Thus, we found that for optimized structures with gain medium layer thicknesses of 543 nm and 1220 nm the required

Optics EXPRESS

material gain coefficients are 9090 cm^{-1} and 4070 cm^{-1}, respectively.

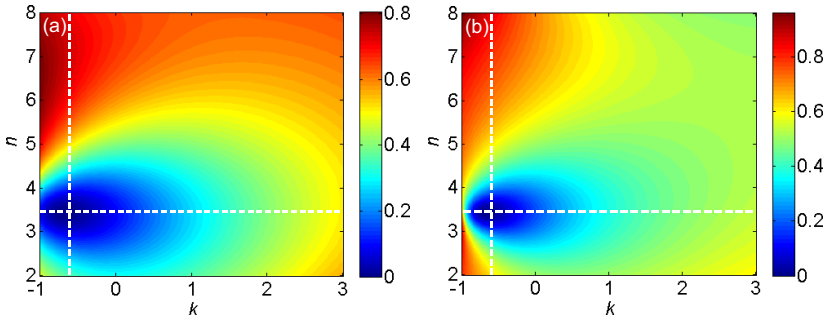

Fig. 5. (a) Calculated reflection for the structure of Fig. 1 with GST in its crystalline phase as a function of the real and imaginary parts, n and k, of the refractive index of the gain material. Results are shown for normal incidence from the backward direction at f = 193.4 THz (λ_0 =1.55 μm). All other parameters are as in Fig. 2(a). The dashed lines correspond to the n and k of the optimized structure ($\tilde{n}_g = n + jk$ = 3.44 - j0.67). (b) Same as in (a) except that GST is in its amorphous phase and results are shown for normal incidence from the forward direction.

3.2. *Exceptional points and their topological properties*

As we discussed in Section 2, in the presence of loss or gain, the optical system of Fig.1 is analogous to open quantum systems which are characterized by complex non-Hermitian Hamiltonians [17–20, 23], and there is a close analogy between optical scattering matrices and Hamiltonian matrices [14, 15, 19, 20, 23]. When the optical scattering matrix eigenvalues coalesce into a single eigenvalue, and the eigenstates coalesce into a single eigenstate, the system exhibits an optical exceptional point [14, 19, 20, 23]. This leads to unidirectional reflectionless propagation in either the forward or the backward direction. In the non-PT-symmetric three-layer system of Fig. 1 with L_1 = 276 nm, L_2 = 84 nm, L_3 = 2 nm, and $k = -0.67$ the existence of exceptional points for GST in both its amorphous and crystalline phases, leads to unidirectional reflectionless propagation in the forward direction ($r_f = 0, r_b \neq 0$) for GST in its amorphous phase, and in the backward direction ($r_b = 0, r_f \neq 0$) for GST in its crystalline phase at f = 193.4 THz (λ_0 =1.55 μm).

In Fig. 6(a), we observe that the phase of the reflection coefficient in the backward direction r_b for the optimized three-layer structure of Fig. 1 with GST in its crystalline phase undergoes an abrupt π jump, when the frequency is crossing over the exceptional point, which actually resembles the phase transition from the PT-symmetric phase to the PT-broken phase in optical PT-symmetric systems [16, 19, 20, 23]. In contrast, the phase of the reflection coefficient in the forward direction r_f varies smoothly with frequency [16, 23]. Similarly, we observe that the phase of the reflection coefficient in the forward direction r_f for the optimized three-layer structure of Fig. 1 with GST in its amorphous phase undergoes an abrupt π jump, while the phase of the reflection coefficient in the backward direction r_b varies smoothly with frequency [Fig. 6(b)].

To gain further insight into the properties of the exceptional point for the non-PT-symmetric system of Fig. 1, we also investigate the topological structure of this exceptional point. In open quantum systems, the eigenvalues of a 2×2 non-Hermitian matrix can be expanded in Puiseux series around exceptional points [1]. In the vicinity of an exceptional point, the two complex eigenvalues are almost degenerate and can be approximated as [1]

$$E_{\pm}(x) = E_{EP} \pm \alpha\sqrt{x - x_{EP}}, \tag{3}$$

Optics EXPRESS

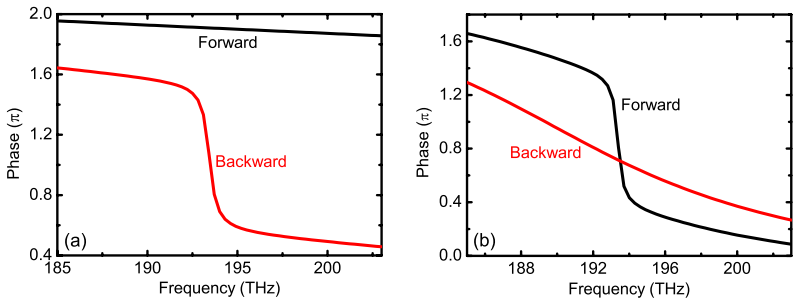

Fig. 6. (a) Phase spectra of the reflection coefficients in the forward (r_f, black) and backward (r_b, red) directions for the structure of Fig. 1 with GST in its crystalline phase. All parameters are as in Fig. 2(a). (b) Same as in (a) except that GST is in its amorphous phase.

where $E_{\pm}(x)$ and x_{EP} are the eigenvalues and the corresponding exceptional point for the 2×2 non-Hermitian matrix in parameter x space, respectively, and α is complex. When $x - x_{EP} < 0$, the coefficient α has to be multiplied by a factor of $j = e^{j\frac{\pi}{2}}$, compared to the case of $x - x_{EP} > 0$. Thus, as the parameter x increases in the interval $[x_{EP} - \delta, x_{EP} + \delta]$, where δ is sufficiently small, the two eigenvalues for $x - x_{EP} < 0$ should move along a line which is perpendicular to that for $x - x_{EP} > 0$ [1,2].

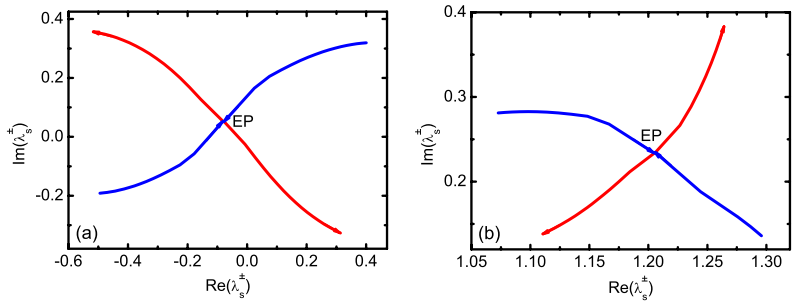

Fig. 7. (a) Schematic representation of the coalescence of the two eigenvalues $\lambda_s^{\pm}$ of the scattering matrix $\mathbf{S}$ [Eq. (1)], as the thickness L_2 is varied for the structure of Fig. 1 with GST in its crystalline phase. The red lines correspond to the eigenvalues for $L_2 \geqq 84$ nm, the blue lines correspond to the eigenvalues for $L_2 < 84$ nm, and the meeting-point of the arrows corresponds to the exceptional point. Results are shown for $f = 193.4$ THz (λ_0 =1.55 μm). All other parameters are as in Fig. 2(a). (b) Same as in (a) except that GST is in its amorphous phase.

Figure 7(a) shows the trajectories of the two eigenvalues $\lambda_s^{\pm}$ of the scattering matrix $\mathbf{S}$ [Eq. (1)] for the optimized structure of Fig. 1 with GST in its crystalline phase as the thickness L_2 approaches the exceptional point ($L_2 = 84$ nm). We observe that for $L_2 < 84$ nm the two eigenvalues first move along the blue lines as L_2 increases, and coalesce at the exceptional point for $L_2 = 84$ nm. As L_2 further increases ($L_2 > 84$ nm), the two degenerate eigenvalues are split again and move along the red lines which are indeed perpendicular to the blue ones around the exceptional point. Figure 7(b) shows the trajectories of the two eigenvalues $\lambda_s^{\pm}$ for the optimized structure of Fig. 1 with GST in its amorphous phase. Similarly, we observe that the two eigenvalues coalesce at the exceptional point, and the angle between the in and out trajectories around the exceptional point is $\sim 90^{\circ}$ in the complex eigenvalue plane, when L_2 sweeps over the exceptional point.

Another unique topological property of exceptional points is that, when encircling an exceptional

Optics EXPRESS

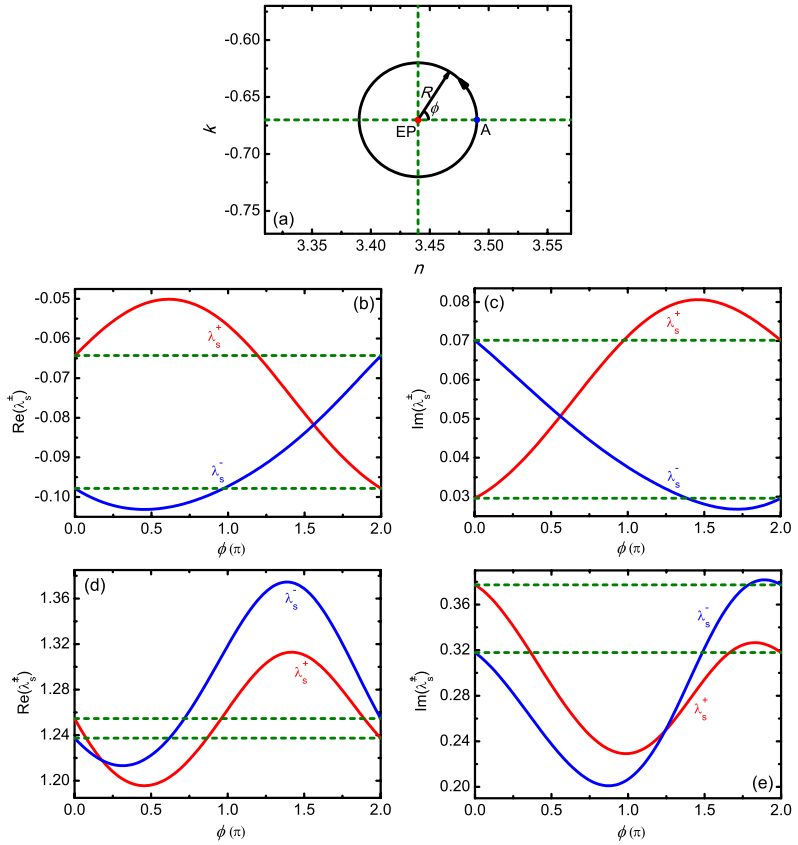

Fig. 8. (a) A circular loop in the parameter space of the real and imaginary parts, n and k, of the complex refractive index of the gain material. The circle is centered at the exceptional point (red dot with $\tilde{n}_g = 3.44 - j0.67$), and its radius R is set to be 0.05. The blue dot represents the starting position of the loop (point A with $\tilde{n}_g = 3.49 - j0.67$). (b) and (c) The trajectories of the real and imaginary parts of the eigenvalues $\lambda_s^{\pm}$ of the scattering matrix $\mathbf{S}$ [Eq. (1)] for the structure of Fig. 1, as the path of the complex refractive index of the gain material traces the circular loop of Fig. 8(a) in the counterclockwise orientation. Results are shown for GST in its crystalline phase and f = 193.4 THz (λ_0 =1.55 μm). All other parameters are as in Fig. 2(a). (d) and (e). Same as in (b) and (c) except that GST is in its amorphous phase.

point in parameter space, the eigenvalues will be interchanged after a complete loop, because of the square root behavior of the singularity [1, 2, 65-68]. In our non-PT-symmetric system (Fig. 1), we consider the parameter space of the real and imaginary parts, n and k, of the complex refractive index of the gain material. The exceptional point is encircled by a circular loop with a radius of R in the n-k plane and is located at the center of this circle ($\tilde{n}_{g,EP} = n_{EP} + jk_{EP}$ = 3.44 - j0.67) [Fig. 8(a)]. The radius R is chosen as 0.05 to ensure that only the exceptional point that we obtained by optimizing the structure is embedded inside this circle. We vary the refractive index of the gain material in the counterclockwise direction along the circular loop from the initial position A with $\tilde{n}_g = 3.49 - j0.67$ [Fig. 8(a)]. That is, we vary the refractive index $\tilde{n}_g$ such that

$$\tilde{n}_g - \tilde{n}_{g,EP} = Re^{j\phi}, \tag{4}$$

where ϕ is adiabatically varied from $\phi = 0$ to $\phi = 2\pi$.

Optics EXPRESS

Figures 8(b) and 8(c) show the trajectories of the real and imaginary parts of the eigenvalues $\lambda_s^{\pm}$ of the scattering matrix **S** [Eq. (1)] for the structure of Fig. 1 with GST in its crystalline phase, as the path of the complex refractive index of the gain material traces the circular loop of Fig. 8(a), which encircles the exceptional point, in the counterclockwise orientation. We observe that the two complex eigenvalues are interchanged after one loop of 2π, that is

$$\lambda_s^{\pm}(2\pi) = \lambda_s^{\mp}(0). \tag{5}$$

The interchange of the two eigenvalues further confirms the existence of the exceptional point in the non-*PT*-symmetric system of Fig. 1. Based on Eq. (5), the eigenvalues will return to their original values after two loops with the same orientation, which indicates that the exceptional point is a second order branch point for the eigenvalues [1, 2]. Figures 8(d) and 8(e) also show that the two complex eigenvalues are interchanged after one loop of 2π for the structure of Fig. 1 with GST in its amorphous phase. In contrast, if there is no exceptional point in the closed loop, the eigenvalues will return to themselves at the end of the loop [1, 66]. Note that the switching of the eigenvalues implies the existence of an exceptional point inside the loop. Due to this unique topological structure of exceptional points, the switching of the eigenvalues indicates the existence of the exceptional point inside the loop without the need to locate the exact parameters at which the exceptional point occurs [1, 66, 68].

4. Conclusions

In this paper, we designed a non-*PT*-symmetric three-layer structure, consisting of a gain medium layer sandwiched between two phase-change medium layers for switching of the direction of reflectionless light propagation at exceptional points. We showed that for this structure unidirectional reflectionlessness in the forward direction can be switched to unidirectional reflectionlessness in the backward direction at the optical communication wavelength of $\lambda_0 = 1.55\mu$m by switching the phase-change material GST from its amorphous to its crystalline phase. We used the transfer matrix method and optimized the geometric and material parameters of the structure, to minimize the reflection in the forward direction when GST is in its amorphous phase, and the reflection in the backward direction when GST is in its crystalline phase. We also confirmed these findings with full-wave FDFD simulations. We discussed the underlying physical mechanism of unidirectional reflectionless light propagation in this structure, and the role of the ultrathin GST layer in the reflection process from the structure. We showed that a gain material layer has to be included in the structure in order to compensate the material loss in the GST layers and achieve complete destructive interference.

We also showed that it is the existence of exceptional points for the structure with GST in both its amorphous and crystalline phases which leads to unidirectional reflectionless propagation in the forward direction for GST in its amorphous phase, and in the backward direction for GST in its crystalline phase. We observed that the phase of the reflection coefficient in the direction of reflectionless light propagation undergoes an abrupt π jump, when the frequency is crossing over the exceptional point, which resembles the phase transition from the *PT*-symmetric phase to the *PT*-broken phase in optical *PT*-symmetric systems. We also found that, as the thickness of the gain medium layer is varied, the angle between the in and out trajectories of the two eigenvalues of the scattering matrix of the structure around the exceptional point is $\sim 90^\circ$ in the complex eigenvalue plane. Finally, we investigated the trajectories of the two eigenvalues of the scattering matrix of the structure, as the path of the complex refractive index of the gain material traces a circular loop which encircles the exceptional point, and found that the two eigenvalues are interchanged after one loop of 2π. The interchange of the two eigenvalues further confirms the existence of the exceptional point in the structure.

As final remarks, for experimental realization, an ultrathin thermal barrier layer can be used next to a GST layer to confine heat in the GST film. Such a thermal barrier layer keeps surrounding

Optics EXPRESS

materials isolated from heating and protects them from harmful interaction with the GST film, when GST is switched between its two phases by optically, electrically or thermally provided heat stimuli [35, 40, 45]. For example, Ta_2O_5, Al_2O_3 and Si_3N_4 are materials which can be chosen for the thermal barrier due to their low thermal conductivities [35, 40, 45]. We found that the addition of such a thin thermal barrier layer does not affect the functionality of the proposed structure. In addition, even though the structure was designed assuming normally incident light, we found that the contrast ratio between the forward and backward reflection is large in a wide angular range for both TE and TM polarization, and for GST in both its amorphous and crystalline phases. Our results could be potentially important for developing a new generation of compact active free-space optical devices. It is noteworthy that the concept of combining gain and phase-change materials for switching of the direction of reflectionless light propagation could also be applied to nanoplasmonic waveguide-cavity systems [23, 26], which could lead to implementations in integrated optical chips.

Funding

Foundation of the Key Laboratory of Optoelectronic Devices and Systems of Ministry of Education and Guangdong Province (GD201601); Hunan Provincial Natural Science Foundation of China (2017JJ3375); National Natural Science Foundation of China (NSFC) (61605252, 61422506); National Science Foundation (NSF) (1254934).